AIMS Mathematics, 9(8): 20390–20412.
DOI: 10.3934/math.2024992
Received: 17 March 2024
Revised: 29 April 2024
Accepted: 07 May 2024
Published: 24 June 2024

https://www.aimspress.com/journal/Math

Research article

Unveiling solitons and dynamic patterns for a (3+1)-dimensional model describing nonlinear wave motion

Muhammad Bilal Riaz[1,2,*], **Syeda Sarwat Kazmi**[1], **Adil Jhangeer**[1,3] **and Jan Martinovic**[1]

[1] IT4 Innovations, VSB–Technical University of Ostrava, Ostrava, Czech Republic

[2] Department of Computer Science and Mathematics, Lebanese American University, Byblos, Lebanon

[3] Department of Mathematics, Namal University, Talagang Road, Mianwali 42250, Pakistan

* **Correspondence:** Email: muhammad.bilal.riaz@vsb.cz.

Abstract: In this study, the underlying traits of the new wave equation in extended (3+1) dimensions, utilized in the field of plasma physics and fluids to comprehend nonlinear wave scenarios in various physical systems, were explored. Furthermore, this investigation enhanced comprehension of the characteristics of nonlinear waves present in seas and oceans. The analytical solutions of models under consideration were retrieved using the sub-equation approach and Sardar sub-equation approach. A diverse range of solitons, including bright, dark, combined dark-bright, and periodic singular solitons, was made available through the proposed methods. These solutions were illustrated through visual depictions utilizing 2D, 3D, and density plots with carefully chosen parameters. Subsequently, an analysis of the dynamical nature of the model was undertaken, encompassing various aspects such as bifurcation, chaos, and sensitivity. Bifurcation analysis was conducted via phase portraits at critical points, revealing the system's transition dynamics. Introducing an external periodic force induced chaotic phenomena in the dynamical system, which were visualized through time plots, two-dimensional plots, three-dimensional plots, and the presentation of Lyapunov exponents. Furthermore, the sensitivity analysis of the investigated model was executed utilizing the Runge-Kutta method. The obtained findings indicated the efficacy of the presented approaches for analyzing phase portraits and solitons over a wider range of nonlinear systems.

Keywords: new integrable wave equation; soliton solutions; sub-equation method; Sardar sub-equation method; bifurcation; chaotic behavior; sensitivity
Mathematics Subject Classification: 34H10, 35C08

1. Introduction

In light of its growing significance, researchers have placed a great deal of emphasis on studying nonlinear partial differential equations (NPDEs). Multiple scientific areas, including hydrodynamics, fluids, engineering, and other domains, have made use of these nonlinear equations [1–3]. Many solitary waves associated with NPDEs have been identified in the search for exact solutions, especially in disciplines such as nonlinear optics, quantum physics, plasma, and many others [4–6]. Scholars have centered on solving these NPDEs using different analytical approaches. Among the notable approaches are the sub-equation approach [7], Painlevé test [8], bilinear approach [9], auxiliary equation method [10], modified auxiliary equation method [11, 12], and Lie symmetry approach [13].

The solitons which usually underpin the telecommunication sector are now of special interests. Solitons also matter significantly as they are pivotal for the advancement of computer systems' computing power while they present wide variety of applications. Such applications cover image processing, data analysis, neurology and fluids, among other fields [14, 15]. The dynamics of the solitons have been studied in great deal using a wide range of nonlinear equations including the Fokas-Lenells equation [16], Manakov model [17], Sakovich model [18], Born-Infeld equation [19], Schrödinger equation [20], complex short pulse equation [21], and the Wadati-Konno-Ichikawa equation [22, 23].

The analysis of integrable equations in (3+1) dimensions has been getting greater exposure recently. These equations are vital for deciphering the physics behind a number of industrial and scientific phenomena. This rising demand has led to the development of multiple nonlinear extended equations, among which are the modified Kadomtsev-Petviashvili (KP) equation and the Korteweg-de Vries (KdV) equation.

Akinyemi [24] examined the equation in (2+1) dimensions:

$$A\Omega_{xt} + a\Omega_{xx} + b(\Omega^2)_{xx} + c\Omega_{xxxx} + d\Omega_{yy} = 0, \tag{1.1}$$

and its extended version, comprising two additional linear terms.

$$A\Omega_{xt} + a\Omega_{xx} + b(\Omega^2)_{xx} + c\Omega_{xxxx} + d\Omega_{yy} + e\Omega_{ty} + h\Omega_{tt} = 0, \tag{1.2}$$

here, the constants A, a, b, c, d, e, and h in the given context are unrestricted real values. It is worth highlighting that when $A = e = d = 0$, Eq (1.2) simplifies to the Boussinesq equation.

$$\Omega_{tt} + a\Omega_{xx} + b(\Omega^2)_{xx} + c\Omega_{xxxx} = 0. \tag{1.3}$$

Equations (1.1) and (1.2) have been demonstrated to exhibit Painlevé integrability, and their multiple solitons have also been obtained [24]. In the ongoing study, our intention is to address an extended version of Eq (1.2) [25].

$$\Omega_{xt} + a\Omega_{xx} + b(\Omega^2)_{xx} + c\Omega_{xxxx} + d\Omega_{yy} + e\Omega_{ty} + h\Omega_{tt} + k\Omega_{xy} + m\Omega_{xz} = 0, \tag{1.4}$$

where $\Omega = \Omega(x, y, z, t)$. It is evident that Eq (1.4) is constructed by introducing two additional linear terms, specifically $k\Omega_{xy}$, and $m\Omega_{xz}$ to Eq (1.2). Furthermore, the coefficients a, b, c, d, e, h, k and m are random real values. Wazwaz et al. [25] investigated the integrability criteria for the discussed

model (1.4) through the use of the Painlevé test. The study concluded by analyzing a set of lump solutions for the suggested equation. The suggested model is designed to aid numerous researchers engaged in plasma physics and fluid mechanics by providing insights into the characteristics of nonlinear waves occurring in various physical systems. Furthermore, this investigation will enhance comprehension of the characteristics of nonlinear waves present in seas and oceans.

In this study, we undertake a comprehensive exploration of a nonlinear model (1.4), employing two distinct but complementary methodologies: the sub-equation (SE) approach [7], and the Sardar sub-equation (SSE) approach [26]. The SE approach yields results expressed in trigonometric and hyperbolic functions. To deepen our understanding of the equation, we introduce the SSE approach alongside the SE approach. The SSE approach, an extension of the SE approach, emerges as an effective analytical tool for extracting precise solutions from nonlinear models. By employing the SSE technique, bright, dark, dark-bright (combo), and periodic solitons are discovered and visually portrayed using density plots, two dimensional and three dimensional plots. It is notable that Eq (1.4) has never been addressed using the techniques outlined in this paper. The results of this study expand theoretical comprehension in the domain of NPDEs.

A rising tide of attention has been devoted in recent years to the analysis of differential equation (DE) dynamics via the facets of chaos and bifurcation. Dynamical systems find wide-ranging applications in several domains, including economics, engineering, and biology [27, 28]. Bifurcation analysis studies how an orbit evolves with respect to distinct parameters. Moreover, there has been a noticeable emphasis on studying NPDEs when an outside periodic disturbance is involved. This focus has led due to the realization that a fully integrable nonlinear model falls short in clarifying quasi-periodic and chaotic features. On the contrary, these irregular patterns may be elicited by applying an outward periodic disturbance to a nonlinear system. For instance, in their work, Riaz et al. [28] investigated the dynamics of bifurcation, chaos, and solitons for the oskolkov equation. Similarly, Rafiq et al. [29] studied the dynamic nature of shallow equations, and extracted the multi-wave solitons. Furthermore, the study conducted by Hosseini et al. [30] concentrated on examining the sensitive and dynamic features of the Schrödinger equation. In this work, we studied the chaotic phenomena of the discussed equation through the presentation of two-dimensional plots, three-dimensional plots, time plots, and Lyapunov exponents.

• Phase plots offer a graphic depiction of a planar system's characteristics. They involve plotting one state variable against another. Examining the structure of the resultant graph can furnish valuable insights into the system's dynamics, encompassing aspects such as periodicity, or inclination towards chaos.

• A time plot refers to a set of points that are systematically accumulated over a specific time span. In this method, the state variables of system undergo scrutiny, and if they exhibit irregular patterns, they are classified as chaotic. Conversely, if these variables manifest periodicity, or quasi-periodic tendencies, they are categorized as non-chaotic.

• Lyapunov exponents (LE) measure how a dynamic system reacts to changes in its initial conditions, assessing the extent to which nearby trajectories either diverge or converge as time progresses. Chaotic behavior is indicated by positive Lyapunov exponents, whereas negative exponents signify stability. Through the computation of LE, we can ascertain whether a system demonstrates chaotic feature or maintains a stable state.

These principles are widely applied in analyzing intricate systems across diverse fields, offering

valuable insights into their dynamics, stability, and behavioral patterns. This research concentrates on exploring a newly extended equation within a (3+1)-dimensional framework, examining it from various perspectives. We employ the sub-equation and Sardar sub-equation techniques to derive analytical solutions, investigate bifurcations at equilibrium points, utilize various chaos detection methods to pinpoint chaotic behavior, and explore the sensitivity of the discussed model. Based on our comprehension, this study seems to be an innovative contribution not previously encountered in the available literature.

The structure of the manuscript is as follows: In Section 2, the description of SE method and SSE method has been given. The mathematical analysis and the application of SE and SSE approaches for finding soliton solutions of the model is presented in Section 3. Results obtained from the analysis are discussed in Section 4. A comprehensive investigation of the dynamic characteristics of the proposed equation, utilizing phase portraits of bifurcation, is conducted in Section 5. Chaotic phenomena is explored in Section 6. In Section 7, sensitivity of the suggested equation is presented. Finally, the conclusion is provided in the last section.

2. Description of proposed methods

In this section, two analytical techniques are examined: the SSE approach and the SE approach. The detail description of the proposed techniques is given in this segment.

Step 1. Let us consider the NPDE as follows:

$$\mathcal{P}(\Omega, \Omega_t, \Omega_x, \Omega_y, \Omega_z, \Omega_{xx}, \Omega_{tt}, ...) = 0. \tag{2.1}$$

Then, using the transformation $\Omega(x, y, z, t) = \Psi(\gamma_1 x + \gamma_2 y + \gamma_3 z + \mu t)$, Eq (2.1) is changed into an ordinary DE as shown:

$$\mathcal{E} = (\Psi, \Psi', \Psi'', ...) = 0. \tag{2.2}$$

Step 2. The initial solution for these approaches is outlined below:

$$\Psi(\zeta) = \sum_{i=0}^{j} \sigma_i \Lambda^i(\zeta), \tag{2.3}$$

here, $\sigma_i, (i = 0, 1, 2, 3, ..., j)$ are random constants to be resolved.

2.1. Description of the SE approach

In this method, the function $\Lambda^i(\zeta)$ fulfils the following auxiliary equation,

$$\Lambda^{'}(\zeta) = \beta + \delta\Lambda^2(\zeta), \quad \beta, \delta \in R, \tag{2.4}$$

here, β and δ are random constants to be assessed afterward. Equation (2.4) has the following solutions:

Case 1: If $\chi = \frac{\beta}{\delta} < 0$, then,

$$\begin{aligned} \Lambda_1(\zeta) &= -\sqrt{-\chi}\tanh(\delta\sqrt{-\chi}\zeta), \\ \Lambda_2(\zeta) &= -\sqrt{-\chi}\coth(\delta\sqrt{-\chi}\zeta), \\ \Lambda_3(\zeta) &= -\sqrt{-\chi}\tanh(2\delta\sqrt{-\chi}\zeta) \pm \iota\sqrt{-\chi}\,\mathrm{sech}(2\delta\sqrt{-\chi}\zeta). \end{aligned} \tag{2.5}$$

Case 2: If $\chi = \frac{\beta}{\delta} > 0$, then,

$$\begin{aligned} \Lambda_4(\zeta) &= \sqrt{\chi}\tan(\delta\sqrt{\chi}\zeta), \\ \Lambda_5(\zeta) &= \sqrt{\chi}\cot(\delta\sqrt{\chi}\zeta), \\ \Lambda_6(\zeta) &= \sqrt{\chi}\tan(2\delta\sqrt{\chi}\zeta) \pm \iota\sqrt{\chi}\sec(2\delta\sqrt{\chi}\zeta). \end{aligned} \tag{2.6}$$

Case 3: If $\chi = \frac{\beta}{\delta} = 0$, then,

$$\Lambda_7(\zeta) = -\frac{\delta}{\zeta + \zeta_0}, \quad \zeta_0 \in R. \tag{2.7}$$

2.2. Description of the SSE approach

In this method, the function $\Lambda^i(\zeta)$ fulfils the following auxiliary equation,

$$\Lambda'(\zeta) = \sqrt{\delta + \alpha\Lambda(\zeta)^2 + \lambda\Lambda(\zeta)^4}, \tag{2.8}$$

here, δ, α and λ are constants and Eq (2.8) presents solution as:

Case 1: If $\alpha > 0$ and $\delta = 0$, then

$$\begin{cases} \Lambda_1^{\pm}(\zeta) = \pm\sqrt{-\frac{mn\alpha}{\lambda}}\,\mathrm{sech}_{mn}(\sqrt{\alpha}\zeta), & (\lambda < 0), \\ \Lambda_2^{\pm}(\zeta) = \pm\sqrt{\frac{mn\alpha}{\lambda}}\,\mathrm{csch}_{mn}(\sqrt{\alpha}\zeta), & (\lambda > 0). \end{cases} \tag{2.9}$$

Here, $\mathrm{sech}_{mn}(\zeta) = \frac{2}{me^{\zeta}+ne^{-\zeta}}$, $\mathrm{csch}(\zeta) = \frac{2}{me^{\zeta}-ne^{-\zeta}}$.

Case 2: If $\alpha < 0$, $\lambda > 0$, and $\delta = 0$, then

$$\begin{cases} \Lambda_3^{\pm}(\zeta) = \pm\sqrt{-\frac{mn\alpha}{\lambda}}\,\mathrm{sec}_{mn}(\sqrt{-\alpha}\zeta), \\ \Lambda_4^{\pm}(\zeta) = \pm\sqrt{-\frac{mn\alpha}{\lambda}}\,\mathrm{csc}_{mn}(\sqrt{-\alpha}\zeta). \end{cases} \tag{2.10}$$

Here, $\mathrm{sec}_{mn}(\zeta) = \frac{2}{me^{\iota\zeta}+ne^{-\iota\zeta}}$, $\mathrm{csc}(\zeta) = \frac{2}{me^{\iota\zeta}-ne^{-\iota\zeta}}$.

Case 3: If $\alpha < 0$, $\lambda > 0$ and $\delta = \frac{\alpha^2}{4\lambda}$, then

$$\begin{cases} \Lambda_5^{\pm}(\zeta) = \pm\sqrt{\frac{-\alpha}{2\lambda}}\,\tanh_{mn}(\sqrt{\frac{-\alpha}{2}}\zeta), \\ \Lambda_6^{\pm}(\zeta) = \pm\sqrt{\frac{-\alpha}{2\lambda}}\,\coth_{mn}(\sqrt{\frac{-\alpha}{2}}\zeta), \\ \Lambda_7^{\pm}(\zeta) = \pm\sqrt{\frac{-\alpha}{2\lambda}}\left(\tanh_{mn}(\sqrt{-2\alpha}\zeta) \pm \iota\sqrt{mn}\,\mathrm{sech}_{mn}(\sqrt{-2\alpha}\zeta)\right), \\ \Lambda_8^{\pm}(\zeta) = \pm\sqrt{\frac{-\alpha}{2\lambda}}\left(\coth_{mn}(\sqrt{-2\alpha}\zeta) \pm \sqrt{mn}\,\mathrm{csch}_{mn}(\sqrt{-2\alpha}\zeta)\right), \\ \Lambda_9^{\pm}(\zeta) = \pm\sqrt{\frac{-\alpha}{8\lambda}}\left(\tanh_{mn}(\sqrt{\frac{-\alpha}{8}}\zeta) + \coth_{mn}(\sqrt{\frac{-\alpha}{8}}\zeta)\right). \end{cases} \tag{2.11}$$

Here, $\tanh_{mn}(\zeta) = \frac{me^{\zeta}-ne^{-\zeta}}{me^{\zeta}+ne^{-\zeta}}$, $\coth(\zeta) = \frac{me^{\zeta}+ne^{-\zeta}}{me^{\zeta}-ne^{-\zeta}}$.

Case 4: If $\alpha > 0$, $\lambda > 0$ and $\delta = \frac{\alpha^2}{4\lambda}$, then

$$\begin{cases} \Lambda_{10}^{\pm}(\zeta) = \pm\sqrt{\frac{\alpha}{2\lambda}}\,\tan_{mn}(\sqrt{\frac{\alpha}{2}}\zeta), \\ \Lambda_{11}^{\pm}(\zeta) = \pm\sqrt{\frac{\alpha}{2\lambda}}\,\cot_{mn}(\sqrt{\frac{\alpha}{2}}\zeta), \\ \Lambda_{12}^{\pm}(\zeta) = \pm\sqrt{\frac{\alpha}{2\lambda}}\left(\tan_{mn}(\sqrt{2\alpha}\zeta) \pm \sqrt{mn}\,\sec_{mn}(\sqrt{2\alpha}\zeta)\right), \\ \Lambda_{13}^{\pm}(\zeta) = \pm\sqrt{\frac{\alpha}{2\lambda}}\left(\cot_{mn}(\sqrt{2\alpha}\zeta) \pm \sqrt{mn}\,\csc_{mn}(\sqrt{2\alpha}\zeta)\right), \\ \Lambda_{14}^{\pm}(\zeta) = \pm\sqrt{\frac{\alpha}{8\lambda}}\left(\tan_{mn}(\sqrt{\frac{\alpha}{8}}\zeta) + \cot_{mn}(\sqrt{\frac{\alpha}{8}}\zeta)\right). \end{cases} \tag{2.12}$$

Here, $\tan_{mn}(\zeta) = -\iota\frac{me^{\iota\zeta}-ne^{-\iota\zeta}}{me^{\iota\zeta}+ne^{-\iota\zeta}}$, $\cot(\zeta) = \iota\frac{me^{\iota\zeta}+ne^{-\iota\zeta}}{me^{\iota\zeta}-ne^{-\iota\zeta}}$ with parameters m and n. Upon $m = n = 1$, they become known trigonometric and hyperbolic functions.

Step 3. The positive integer j is determined by homogeneous balance approach.

Step 4. A system of equations for $\Lambda_i's$ are generated by substituting Eq (2.4) from SE approach and Eq (2.8) from SSE approach into Eq (2.2) and reducing the coefficients of Λ^i to zero. To determine the solution of Eq (2.2), we then solve the resulting system using tools like Mathematica.

3. Mathematical analysis

The extended wave equation in (3+1) dimensions can be expressed as:

$$\Omega_{xt} + a\Omega_{xx} + b(\Omega^2)_{xx} + c\Omega_{xxxx} + d\Omega_{yy} + e\Omega_{ty} + h\Omega_{tt} + k\Omega_{xy} + m\Omega_{xz} = 0. \tag{3.1}$$

By assuming the traveling wave transformation as:

$$\Omega(x, y, z, t) = \Psi(\zeta), \quad \zeta = \gamma_1 x + \gamma_2 y + \gamma_3 z + \mu t. \tag{3.2}$$

Here, $\Psi(\zeta)$ and μ represent the characteristics of the traveling wave, specifically referring to its shape and velocity. Additionally, $\gamma_1, \gamma_2, \gamma_3$ serve as random parameters. Upon substituting the expression from Eq (3.2) into Eq (3.1), we obtain the resulting equation.

$$(c\gamma_1^4)\Psi^{(4)} + (\gamma_1\mu + a\gamma_1^2 + d\gamma_2^2 + e\mu\gamma_2 + h\mu^2 + k\gamma_1\gamma_2 + m\gamma_1\gamma_3)\Psi'' + 2b\gamma_1^2\Psi\Psi'' + 2b\gamma_1^2(\Psi')^2 = 0. \tag{3.3}$$

By integrating Eq (3.3) twice with respect to ζ, we acquire;

$$(c\gamma_1^4)\Psi'' + (\gamma_1\mu + a\gamma_1^2 + d\gamma_2^2 + e\mu\gamma_2 + h\mu^2 + k\gamma_1\gamma_2 + m\gamma_1\gamma_3)\Psi + b\gamma_1^2\Psi^2 = 0. \tag{3.4}$$

This section is focused on the application of SSE approach and SE approach for extraction of analytical solutions. By setting Ψ'' equal to Ψ^2 in Eq (3.4), as $j + 2 = 2j$, results $j = 2$.

3.1. Application of the SE approach

This section is focused on the application of SE approach for extraction of analytical solutions. The initial solution in this case becomes:

$$\Psi(\zeta) = \sigma_0 + \sigma_1\Lambda + \sigma_2\Lambda^2. \tag{3.5}$$

Using Eqs (3.5) and (2.4) into Eq (3.4) and solving the resulting system for σ_0, σ_1, σ_2, and a, yields the following solution:

$$\sigma_0 = \frac{-2c\beta\delta\gamma_1^2}{b}, \quad \sigma_1 = 0, \quad \sigma_2 = \frac{-6c\delta^2\gamma_1^2}{b},$$
$$a = \frac{-d\gamma_2^2 - m\gamma_1\gamma_3 - k\gamma_1\gamma_2 - 4c\beta\delta\gamma_1^4 - \mu\gamma_1 - e\mu\gamma_2 - h\mu^2}{\gamma_1^2}. \tag{3.6}$$

By putting above values in Eq (3.5) the solutions of Eq (1.4) are as follows:

Case 1: If $\chi = \frac{\beta}{\delta} < 0$, then,

$$\begin{aligned}
\Omega_1(x,y,z,t) &= \tfrac{-2c\beta\delta\gamma_1^2}{b} - \tfrac{6c\delta^2\gamma_1^2}{b}\Big(-\sqrt{-\chi}\tanh(\delta\sqrt{-\chi}\zeta)\Big)^2,\\
\Omega_2(x,y,z,t) &= \tfrac{-2c\beta\delta\gamma_1^2}{b} - \tfrac{6c\delta^2\gamma_1^2}{b}\Big(-\sqrt{-\chi}\coth(\delta\sqrt{-\chi}\zeta)\Big)^2,\\
\Omega_3(x,y,z,t) &= \tfrac{-2c\beta\delta\gamma_1^2}{b} - \tfrac{6c\delta^2\gamma_1^2}{b}\Big(-\sqrt{-\chi}\tanh(2\delta\sqrt{-\chi}\zeta) \pm \iota\sqrt{-\chi}\,\mathrm{sech}(2\delta\sqrt{-\chi}\zeta)\Big)^2.
\end{aligned} \tag{3.7}$$

Case 2: If $\chi = \frac{\beta}{\delta} > 0$, then,

$$\begin{aligned}
\Omega_4(x,y,z,t) &= \tfrac{-2c\beta\delta\gamma_1^2}{b} - \tfrac{6c\delta^2\gamma_1^2}{b}\Big(\sqrt{\chi}\tan(\delta\sqrt{\chi}\zeta)\Big)^2,\\
\Omega_5(x,y,z,t) &= \tfrac{-2c\beta\delta\gamma_1^2}{b} - \tfrac{6c\delta^2\gamma_1^2}{b}\Big(\sqrt{\chi}\cot(\delta\sqrt{\chi}\zeta)\Big)^2,\\
\Omega_6(x,y,z,t) &= \tfrac{-2c\beta\delta\gamma_1^2}{b} - \tfrac{6c\delta^2\gamma_1^2}{b}\Big(\sqrt{\chi}\tan(2\delta\sqrt{\chi}\zeta) \pm \iota\sqrt{\chi}\sec(2\delta\sqrt{\chi}\zeta)\Big)^2.
\end{aligned} \tag{3.8}$$

Case 3: If $\chi = \frac{\beta}{\delta} = 0$, then,

$$\Omega_7(x,y,z,t) = \frac{-2c\beta\delta\gamma_1^2}{b} - \frac{6c\delta^2\gamma_1^2}{b}\Big(-\frac{\delta}{\zeta+\zeta_0}\Big)^2, \quad \zeta_0 \in R. \tag{3.9}$$

In all above cases $\zeta = \gamma_1 x + \gamma_2 y + \gamma_3 z + \mu t$.

3.2. Application of SSE approach

In this part, we employ the SSE method to solve Eq (3.4). The initial solution for $j = 2$ becomes:

$$\Psi(\zeta) = \sigma_0 + \sigma_1\Lambda + \sigma_2\Lambda^2, \tag{3.10}$$

where σ_0, σ_1, and σ_2 are constants to be extracted. Using Eqs (3.10) and (2.8) into Eq (3.4) and solving the resulting system for σ_0, σ_1, σ_2, and a, yields the following solution:

$$\begin{aligned}
\sigma_0 &= \frac{2\left(-\alpha + \sqrt{\alpha^2 - 3\,\delta\,\lambda}\right){\gamma_1}^2 c}{b}, \quad \sigma_1 = 0, \quad \sigma_2 = -\frac{6c\lambda\,{\gamma_1}^2}{b},\\
a &= -\frac{4\,c{\gamma_1}^4\sqrt{\alpha^2 - 3\,\delta\,\lambda} + d{\gamma_2}^2 + e\mu\,\gamma_2 + h\mu^2 + k\gamma_1\gamma_2 + m\gamma_3\gamma_1 + \gamma_1\mu}{{\gamma_1}^2}.
\end{aligned} \tag{3.11}$$

By putting above values in Eq (3.10) the solutions of Eq (1.4) are as follows:

Case 1: If $\alpha > 0$ and $\delta = 0$, then

$$\begin{cases}
\Omega_1^{\pm}(x,y,z,t) = \frac{2\left(-\alpha+\sqrt{\alpha^2-3\,\delta\,\lambda}\right){\gamma_1}^2 c}{b} - \frac{6c\lambda{\gamma_1}^2}{b}\Big(\pm\sqrt{-\frac{mn\alpha}{\lambda}}\,\mathrm{sech}_{mn}(\sqrt{\alpha}\zeta)\Big)^2, & (\lambda < 0),\\
\Omega_2^{\pm}(x,y,z,t) = \frac{2\left(-\alpha+\sqrt{\alpha^2-3\,\delta\,\lambda}\right){\gamma_1}^2 c}{b} - \frac{6c\lambda{\gamma_1}^2}{b}\Big(\pm\sqrt{\frac{mn\alpha}{\lambda}}\,\mathrm{csch}_{mn}(\sqrt{\alpha}\zeta)\Big)^2, & (\lambda > 0).
\end{cases} \tag{3.12}$$

Case 2: If $\alpha < 0$, $\lambda > 0$, and $\delta = 0$, then

$$\begin{cases} \Omega_3^{\pm}(x,y,z,t) = \frac{2\left(-\alpha+\sqrt{\alpha^2-3\,\delta\,\lambda}\right)\gamma_1{}^2 c}{b} - \frac{6c\lambda\,\gamma_1{}^2}{b}\left(\pm\sqrt{-\frac{mn\alpha}{\lambda}}\,\mathrm{sec}_{mn}(\sqrt{-\alpha}\zeta)\right)^2, \\ \Omega_4^{\pm}(x,y,z,t) = \frac{2\left(-\alpha+\sqrt{\alpha^2-3\,\delta\,\lambda}\right)\gamma_1{}^2 c}{b} - \frac{6c\lambda\,\gamma_1{}^2}{b}\left(\pm\sqrt{-\frac{mn\alpha}{\lambda}}\,\mathrm{csc}_{mn}(\sqrt{-\alpha}\zeta)\right)^2. \end{cases} \tag{3.13}$$

Case 3: If $\alpha < 0$, $\lambda > 0$ and $\delta = \frac{\alpha^2}{4\lambda}$, then

$$\begin{cases} \Omega_5^{\pm}(x,y,z,t) = \frac{2\left(-\alpha+\sqrt{\alpha^2-3\,\delta\,\lambda}\right)\gamma_1{}^2 c}{b} - \frac{6c\lambda\,\gamma_1{}^2}{b}\left(\sqrt{\frac{-\alpha}{2\lambda}}\,\tanh_{mn}(\sqrt{\frac{-\alpha}{2}}\zeta)\right)^2, \\ \Omega_6^{\pm}(x,y,z,t) = \frac{2\left(-\alpha+\sqrt{\alpha^2-3\,\delta\,\lambda}\right)\gamma_1{}^2 c}{b} - \frac{6c\lambda\,\gamma_1{}^2}{b}\left(\sqrt{\frac{-\alpha}{2\lambda}}\,\coth_{mn}(\sqrt{\frac{-\alpha}{2}}\zeta)\right)^2, \\ \Omega_7^{\pm}(x,y,z,t) = \frac{2\left(-\alpha+\sqrt{\alpha^2-3\,\delta\,\lambda}\right)\gamma_1{}^2 c}{b} - \frac{6c\lambda\,\gamma_1{}^2}{b}\left(\sqrt{\frac{-\alpha}{2\lambda}}\left(\tanh_{mn}(\sqrt{-2\alpha}\zeta) \pm \iota\sqrt{mn}\,\mathrm{sech}_{mn}(\sqrt{-2\alpha}\zeta)\right)\right)^2, \\ \Omega_8^{\pm}(x,y,z,t) = \frac{2\left(-\alpha+\sqrt{\alpha^2-3\,\delta\,\lambda}\right)\gamma_1{}^2 c}{b} - \frac{6c\lambda\,\gamma_1{}^2}{b}\left(\sqrt{\frac{-\alpha}{2\lambda}}\left(\coth_{mn}(\sqrt{-2\alpha}\zeta) \pm \sqrt{mn}\,\mathrm{csch}_{mn}(\sqrt{-2\alpha}\zeta)\right)\right)^2, \\ \Omega_9^{\pm}(x,y,z,t) = \frac{2\left(-\alpha+\sqrt{\alpha^2-3\,\delta\,\lambda}\right)\gamma_1{}^2 c}{b} - \frac{6c\lambda\,\gamma_1{}^2}{b}\left(\pm\sqrt{\frac{-\alpha}{8\lambda}}\left(\tanh_{mn}(\sqrt{\frac{-\alpha}{8}}\zeta) + \coth_{mn}(\sqrt{\frac{-\alpha}{8}}\zeta)\right)\right)^2. \end{cases} \tag{3.14}$$

Case 4: If $\alpha > 0$, $\lambda > 0$ and $\delta = \frac{\alpha^2}{4\lambda}$, then

$$\begin{cases} \Omega_{10}^{\pm}(x,y,z,t) = \frac{2\left(-\alpha+\sqrt{\alpha^2-3\,\delta\,\lambda}\right)\gamma_1{}^2 c}{b} - \frac{6c\lambda\,\gamma_1{}^2}{b}\left(\sqrt{\frac{\alpha}{2\lambda}}\,\tan_{mn}(\sqrt{\frac{\alpha}{2}}\zeta)\right)^2, \\ \Omega_{11}^{\pm}(x,y,z,t) = \frac{2\left(-\alpha+\sqrt{\alpha^2-3\,\delta\,\lambda}\right)\gamma_1{}^2 c}{b} - \frac{6c\lambda\,\gamma_1{}^2}{b}\left(\sqrt{\frac{\alpha}{2\lambda}}\,\cot_{mn}(\sqrt{\frac{\alpha}{2}}\zeta)\right)^2, \\ \Omega_{12}^{\pm}(x,y,z,t) = \frac{2\left(-\alpha+\sqrt{\alpha^2-3\,\delta\,\lambda}\right)\gamma_1{}^2 c}{b} - \frac{6c\lambda\,\gamma_1{}^2}{b}\left(\sqrt{\frac{\alpha}{2\lambda}}\left(\tan_{mn}(\sqrt{2\alpha}\zeta) \pm \sqrt{mn}\,\mathrm{sec}_{mn}(\sqrt{2\alpha}\zeta)\right)\right)^2, \\ \Omega_{13}^{\pm}(x,y,z,t) = \frac{2\left(-\alpha+\sqrt{\alpha^2-3\,\delta\,\lambda}\right)\gamma_1{}^2 c}{b} - \frac{6c\lambda\,\gamma_1{}^2}{b}\left(\sqrt{\frac{\alpha}{2\lambda}}\left(\cot_{mn}(\sqrt{2\alpha}\zeta) \pm \sqrt{mn}\,\mathrm{csc}_{mn}(\sqrt{2\alpha}\zeta)\right)\right)^2, \\ \Omega_{14}^{\pm}(x,y,z,t) = \frac{2\left(-\alpha+\sqrt{\alpha^2-3\,\delta\,\lambda}\right)\gamma_1{}^2 c}{b} - \frac{6c\lambda\,\gamma_1{}^2}{b}\left(\sqrt{\frac{\alpha}{8\lambda}}\left(\tan_{mn}(\sqrt{\frac{\alpha}{8}}\zeta) + \cot_{mn}(\sqrt{\frac{\alpha}{8}}\zeta)\right)\right)^2. \end{cases} \tag{3.15}$$

In all above cases $\zeta = \gamma_1 x + \gamma_2 y + \gamma_3 z + \mu t$.

4. Results and discussions

In this part, we analyze the attributes of a varied set of acquired solutions. The first portion examines the solutions to the proposed equation utilizing the SE method, whereas the subsequent section investigates solutions to the suggested equation employing the SSE method. The visualization of the results was conducted through three-dimensional, density, and two-dimensional plots. It is important to highlight that within the suggested model, the velocity wave, μ, exhibits two unique values, signifying the existence of dual-wave propagation within the nonlinear system, known as the left-wave and right-wave, both propagating simultaneously.

4.1. Solutions by sub-equation approach

Initially, an array of soliton structures is generated by employing distinct parameter values through the use of the SE technique. Furthermore, employing suitable parameter values has led to the

observation of various distinct structures, including bright solitons, dark solitons, dark-bright(combo) solitons, and singular periodic solitons. In Figure 1, the solution $\Omega_1(x, y, z, t)$ is visually represented as a bright soliton, where the central region exhibits higher intensity while the surrounding area displays lower intensity. The parameter values for this representation are as follows: $\gamma_1 = \gamma_2 = \gamma_3 = b = 1$, $c = -1$, $\beta = 0.1$, $\delta = -0.2$, $z = 1.5$, $t = 2.1$, and $\mu = 1.5$. Moving to Figure 2, a 3D, density, and 2D visualization of $\Omega_1(x, y, z, t)$ is presented with a modified parameter $c = 1$, while all other parameters remain the same as in the previous case, resulting in a recorded dark soliton identified by a localized depression in the surrounding field. Dark solitons, which attract significant attention in optics due to their stable transmission, are highlighted. Shifting to Figure 3, the solution $|\Omega_3(x, y, z, t)|$ is depicted as a dark-bright (combo) soliton, along with its 2D and density plots. Dark-bright solitons combine both dark and bright features within their structure, featuring a localized region of decreased intensity (dark soliton) embedded within a localized region of increased intensity (bright soliton). The parameter values for this scenario are: $\gamma_1 = \gamma_2 = \gamma_3 = b = c = 1$, $\beta = 0.1$, $\delta = -2$, $y = 0.5$, $t = 0.1$, and $\mu = 1.5$. In Figure 4, the solution $|\Omega_6(x, y, z, t)|$ is presented with the following parameters: $\gamma_1 = \gamma_2 = \gamma_3 = b = c = 1$, $\beta = 2.1$, $\delta = 0.2$, $y = 0.5$, $t = 0.1$, resulting in singular periodic solitons displaying discontinuity at the lower ends.

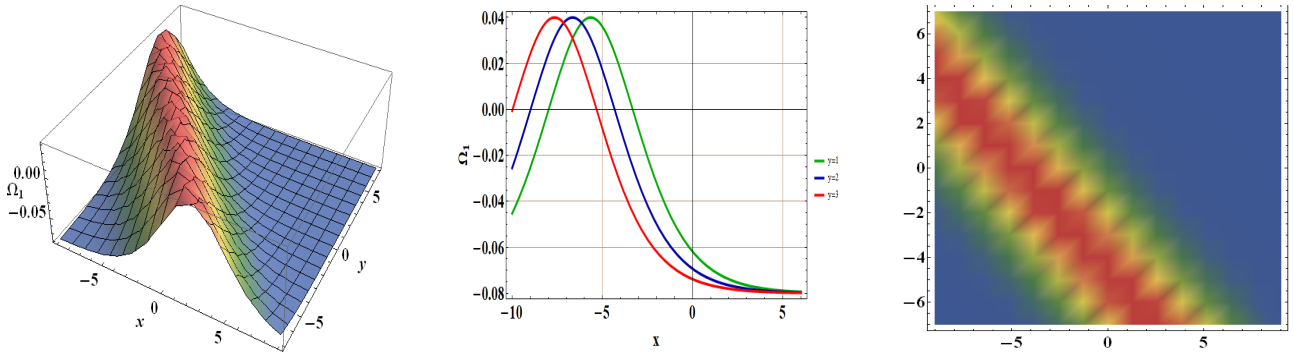

(a) 3D Plot **(b)** 2D Plot **(c)** Density Plot

Figure 1. Visual representation of the solution $\Omega_1(x, y, z, t)$ through 3-dimensional, 2-dimensional and density plots.

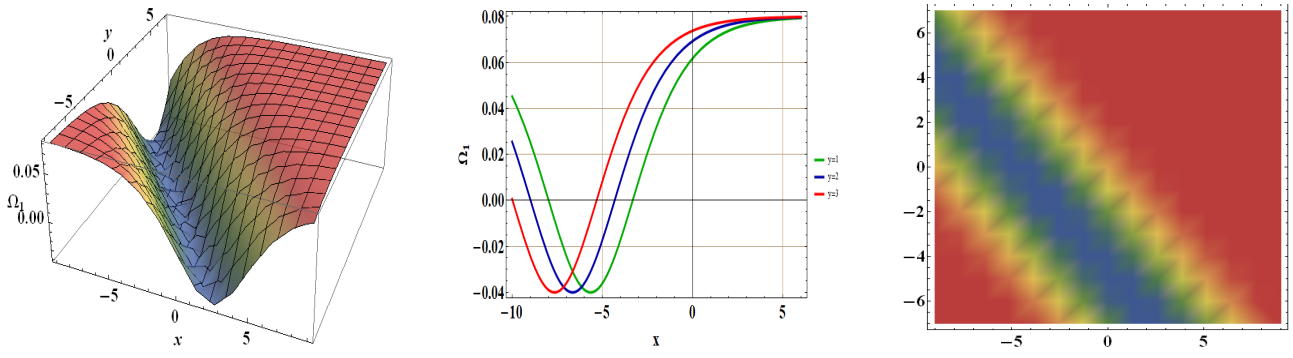

(a) 3D Plot **(b)** 2D Plot **(c)** Density Plot

Figure 2. Visual representation of the solution $\Omega_1(x, y, z, t)$ through 3-dimensional, 2-dimensional and density plots.

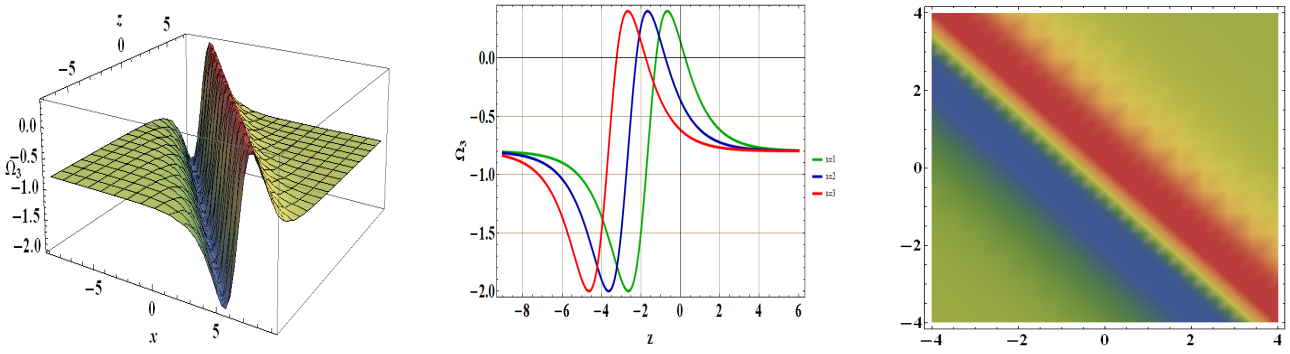

(a) 3D Plot **(b)** 2D Plot **(c)** Density Plot

Figure 3. Visual representation of the solution $\Omega_3(x, y, z, t)$ through 3-dimensional, 2-dimensional and density plots.

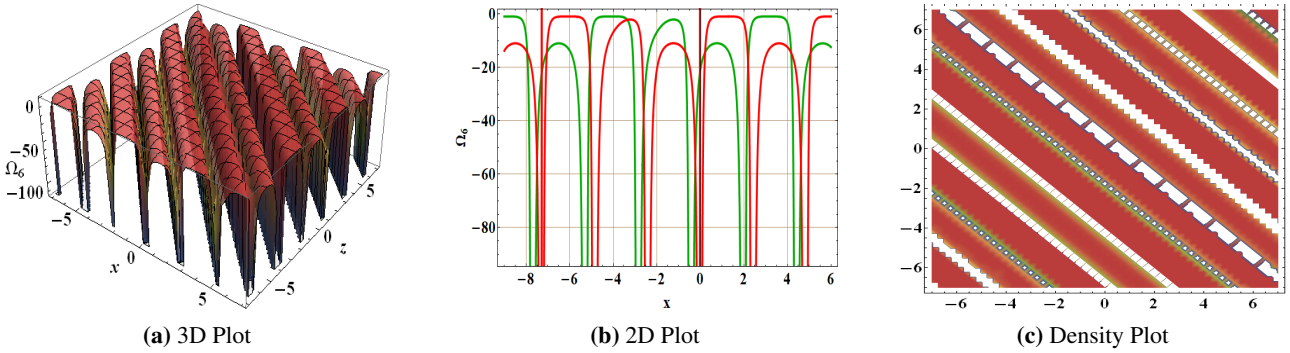

(a) 3D Plot **(b)** 2D Plot **(c)** Density Plot

Figure 4. Visual representation of the solution $\Omega_6(x, y, z, t)$ through 3-dimensional, 2-dimensional and density plots.

4.2. Solutions by Sardar sub-equation approach

Second, diverse soliton structures are produced by employing distinct parameter values for each outcome through the utilization of the SSE technique. Figure 5 illustrates a bright soliton, where the central region exhibits higher intensity while the surrounding area displays lower intensity, along with its 2D and density plot, for the solution $|\Omega_1^{\pm}(x, y, z, t)|$ with the following parametric values: $\gamma_1 = \gamma_2 = \gamma_3 = b = c = 1$, $\alpha = 2$, $\delta = 0$, $\lambda = -1$, $m = 2$, $n = 1.5$, $y = 0.5$, $z = 1$ and $\mu = 1$. In Figure 6, dark soliton, identified by a localized depression in the surrounding field along with its 2D and density plot, is presented for the solution $|\Omega_3^{\pm}(x, y, z, t)|$ with the parametric value $\gamma_1 = \gamma_2 = \gamma_3 = b = 1$, $c = -1$, $\alpha = -0.2$, $\delta = 0$, $\lambda = 0.5$, $m = 1.1$, $n = 1.1$, $y = 0.5$, $z = 1$ and $\mu = 1.5$. Bright solitons, manifesting as concentrated intensity peaks amid a uniform background are showcased in Figure 7 for the solution $|\Omega_5^{\pm}(x, y, z, t)|$ with the parametric values: $\gamma_1 = \gamma_2 = \gamma_3 = b = c = 1$, $\alpha = -2$, $\delta = 1$, $\lambda = 1$, $m = 2$, $n = 1.1$, $x = 0.5$, $z = 1$ and $\mu = 1$. Figure 8 presents combo solitons for the solution $|\Omega_7^{\pm}(x, y, z, t)|$ with the same parametric values as in previous case. Dark-bright solitons combine both dark and bright features within their structure, featuring a localized region of decreased intensity (dark soliton) embedded within a localized region of increased intensity (bright soliton). Periodic solitons are reported in Figure 9 for the solution $|\Omega_{12}^{\pm}(x, y, z, t)|$ with the parametric

values: $\gamma_1 = \gamma_2 = \gamma_3 = b = c = 1$, $\alpha = 2$, $\delta = 1$, $\lambda = 1$, $m = 2$, $n = 1.1$, $x = 0.5$, $z = 1$ and $\mu = 0.5$. These solutions demonstrate a repetitive structure.

These visual depictions offer insights into the unique forms and attributes of diverse soliton solutions. Solitons possess a remarkable quality in their resilience, a crucial aspect ensuring their practical utility in optical communications. Moreover, these solutions showcase the ability to preserve both their form and speed during extensive distances without dispersing or dissipating energy, rendering them optimal for data transmission via optical fibers. They facilitate high-speed, long-range communication with minimal distortion, playing an essential role in today's telecommunications landscape. Thanks to soliton technology, various social media platforms such as Twitter, Instagram, Facebook, LinkedIn, email services, cell phones, and the internet enable seamless collaborations. Additionally, soliton technology facilitates communication across continents and oceans. Examining these solutions enables researchers to enhance their comprehension of the dynamics and traits exhibited by solitons in nonlinear models.

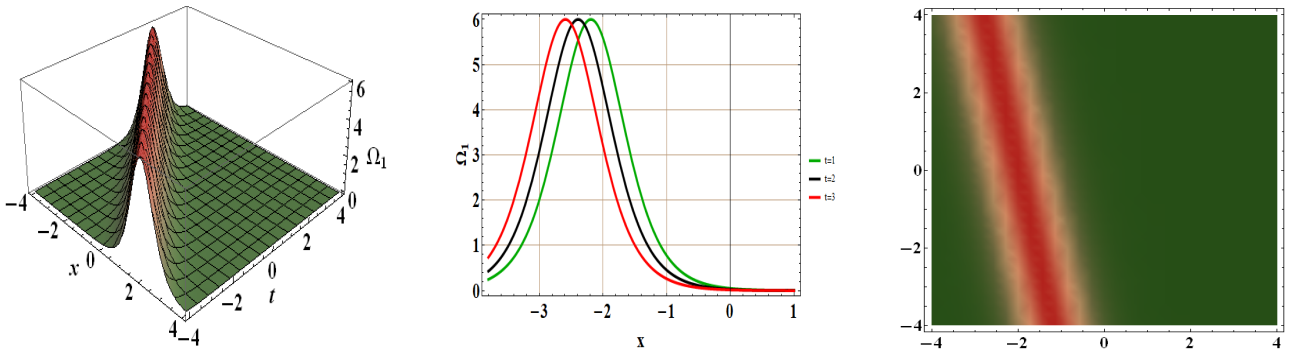

(a) 3D Plot **(b)** 2D Plot **(c)** Density Plot

Figure 5. Visual representation of the solution $|\Omega_1^{\pm}(x, y, z, t)|$ through 3-dimensional, 2-dimensional and density plots.

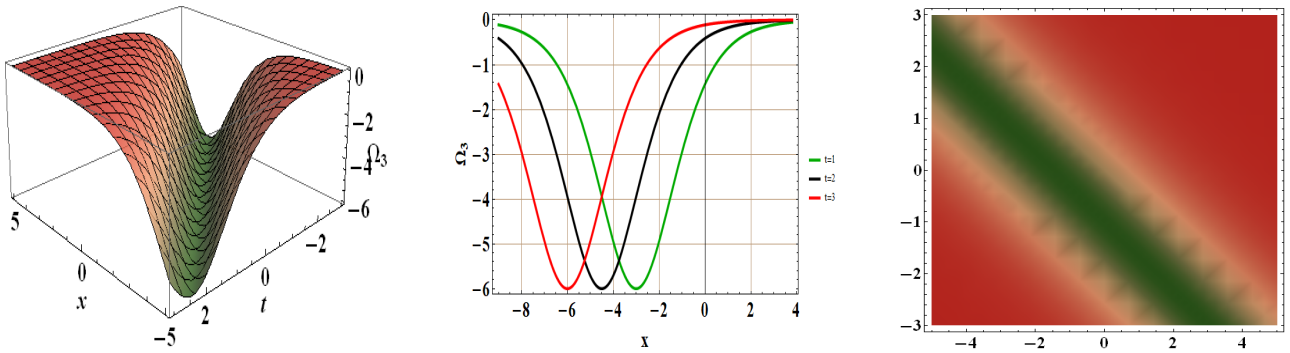

(a) 3D Plot **(b)** 2D Plot **(c)** Density Plot

Figure 6. Visual representation of the solution $|\Omega_3^{\pm}(x, y, z, t)|$ through 3-dimensional, 2-dimensional and density plots.

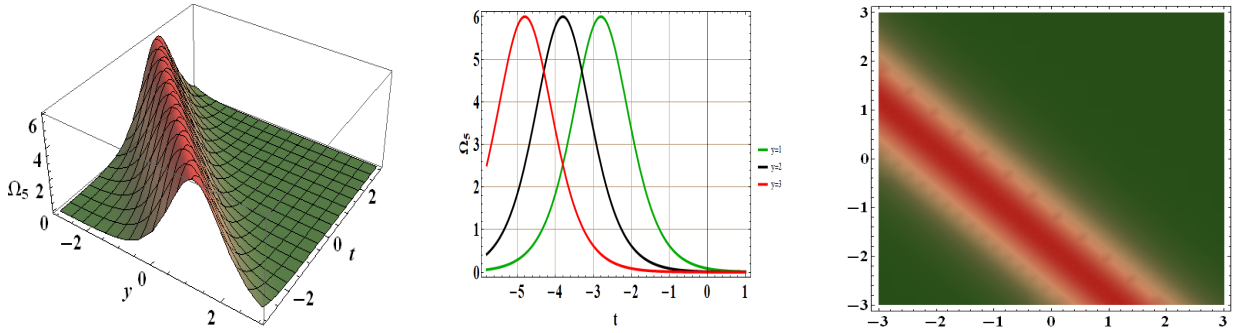

(a) 3D Plot **(b)** 2D Plot **(c)** Density Plot

Figure 7. Visual representation of the solution $|\Omega_5^{\pm}(x, y, z, t)|$ through 3-dimensional, 2-dimensional and density plots.

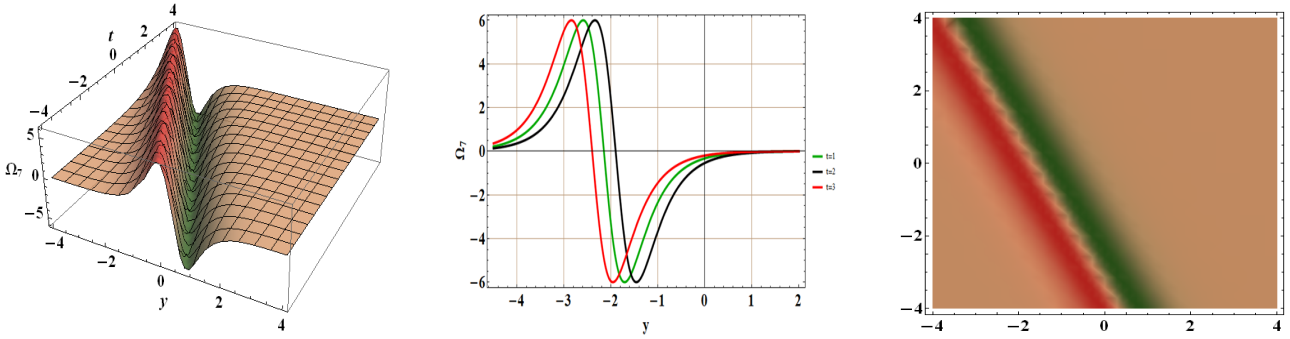

(a) 3D Plot **(b)** 2D Plot **(c)** Density Plot

Figure 8. Visual representation of the solution $|\Omega_7^{\pm}(x, y, z, t)|$ through 3-dimensional, 2-dimensional and density plots.

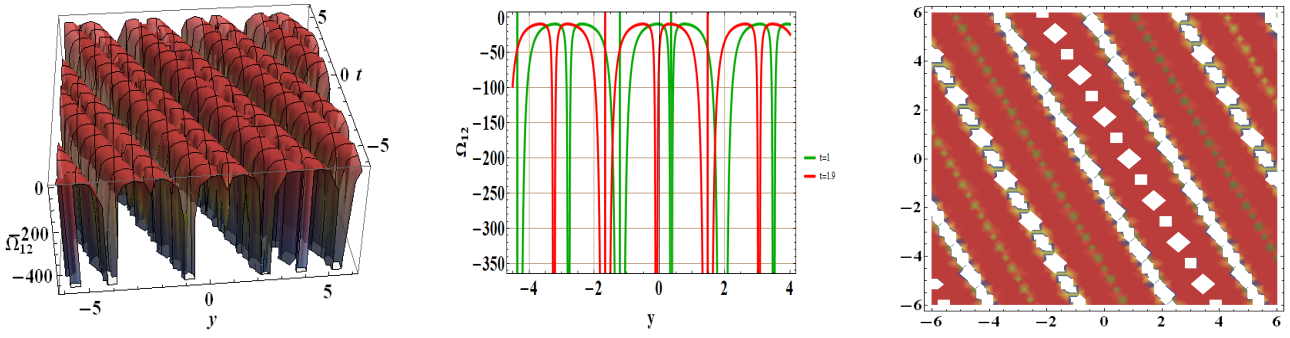

(a) 3D Plot **(b)** 2D Plot **(c)** Density Plot

Figure 9. Visual representation of the solution $|\Omega_{12}^{\pm}(x, y, z, t)|$ through 3-dimensional, 2-dimensional and density plots.

5. Bifurcation phenomena

In this segment, we will analyze Eq (1.4) within the framework of bifurcation analysis [31]. Upon employing the Galilean transformation to Eq (3.4), we derive the planar system as follows:

$$\begin{cases} \frac{d\Psi}{d\zeta} = \Gamma, \\ \frac{d\Gamma}{d\zeta} = -\varpi_0\Psi - \varpi_1\Psi^2, \end{cases} \tag{5.1}$$

where

$$\varpi_0 = \frac{(\gamma_1\mu + a\gamma_1^2 + d\gamma_2^2 + e\mu\gamma_2 + h\mu^2 + k\gamma_1\gamma_2 + m\gamma_1\gamma_3)}{c\gamma_1^4}, \quad \varpi_1 = \frac{b}{c\gamma_1^2}.$$

The Hamiltonian of (5.1), is expressed as follows:

$$\mathcal{H}(\Psi, \Gamma) = \frac{\Gamma^2}{2} + \varpi_0\frac{\Psi^2}{2} + \varpi_1\frac{\Psi^3}{3}, \tag{5.2}$$

which satisfies

$$\frac{\partial\mathcal{H}}{\partial\Psi} = -\Gamma', \quad \frac{\partial\mathcal{H}}{\partial\Gamma} = \Psi'.$$

Examining the dynamic characteristics of (5.1) at its fixed points $\mathcal{F}_j$ (where $j = 1, 2$) using bifurcation theory. The fixed points for (5.1) are outlined below:

$$\mathcal{F}_1 = (0, 0), \mathcal{F}_2 = (\frac{-\varpi_0}{\varpi_1}, 0).$$

Furthermore, the Jacobian of the system will be:

$$\mathcal{J}(\Psi, \Gamma) = \begin{pmatrix} 0 & 1 \\ -\varpi_0 - 2\varpi_1\Psi & 0 \end{pmatrix}. \tag{5.3}$$

The determinant and trace of (5.3) at the critical point $\mathcal{F}_j$ are indicated by $\mathcal{D}$ and $\mathcal{T}$, respectively, and these values are provided as follows:

$$\mathcal{T} = trace(\mathcal{J})|_{\mathcal{F}_j} = 0, \quad \mathcal{D} = det(\mathcal{J})|_{\mathcal{F}_j} = \varpi_0 + 2\varpi_1\Psi.$$

The fixed point is classified as a saddle when $\mathcal{D} < 0$, a central point when $\mathcal{D} > 0$ and $\mathcal{T} = 0$, a cusp when $\mathcal{D} = 0$, and a node if $\mathcal{D} > 0$ and $\mathcal{T}^2 - 4\mathcal{D} > 0$. Varied outcomes can be achieved by adjusting the parameters.

• **Case 1:** Let $\varpi_0 > 0$, and $\varpi_1 > 0$.

For $\gamma_1 = \gamma_2 = \gamma_3 = m = b = a = h = d = \mu = 1, k = e = d = -1$, $\varpi_0 = 1$, and $\varpi_1 = 1$, system (5.1) has two fixed points $\mathcal{F}_1 = (0, 0)$ and $\mathcal{F}_2 = (-1, 0)$. In this case, $\mathcal{F}_1$ is center and $\mathcal{F}_2$ is saddle. These points are presented in Figure 10(a).

• **Case 2:** Let $\varpi_0 < 0$, and $\varpi_1 < 0$.

For $\gamma_1 = \gamma_2 = \gamma_3 = m = c = b = a = h = d = \mu = 1, c = k = e = d = -1$, $\varpi_0 = -1$, and $\varpi_1 = -1$, system (5.1) has two fixed points $\mathcal{F}_1 = (0, 0)$ and $\mathcal{F}_2 = (-1, 0)$. In this case, $\mathcal{F}_1$ is saddle and $\mathcal{F}_2$ is center. These points are presented in Figure 10(b).

• **Case 3:** Let $\varpi_0 < 0$, and $\varpi_1 > 0$.

For $\gamma_1 = \gamma_2 = \gamma_3 = m = b = h = c = \mu = 1, a = k = e = d = -1$, $\varpi_0 = -1$, and $\varpi_1 = 1$, system (5.1) has fixed points as $\mathcal{F}_1 = (0, 0)$ and $\mathcal{F}_2 = (1, 0)$. In this case, $\mathcal{F}_1$ is saddle and $\mathcal{F}_2$ is center. These points are presented in Figure 11(a).

• **Case 4:** Let $\varpi_0 > 0$, and $\varpi_1 < 0$.

For $\gamma_1 = \gamma_2 = \gamma_3 = m = a = h = d = \mu = 1, b = k = e = d = -1$, $\sigma_0 = 1$, and $\sigma_1 = -1$, system (5.1) has fixed points as $\mathcal{F}_1 = (0, 0)$ and $\mathcal{F}_2 = (1, 0)$. In this case, $\mathcal{F}_1$ is center and $\mathcal{F}_2$ is saddle. These points are presented in Figutr 11(b).

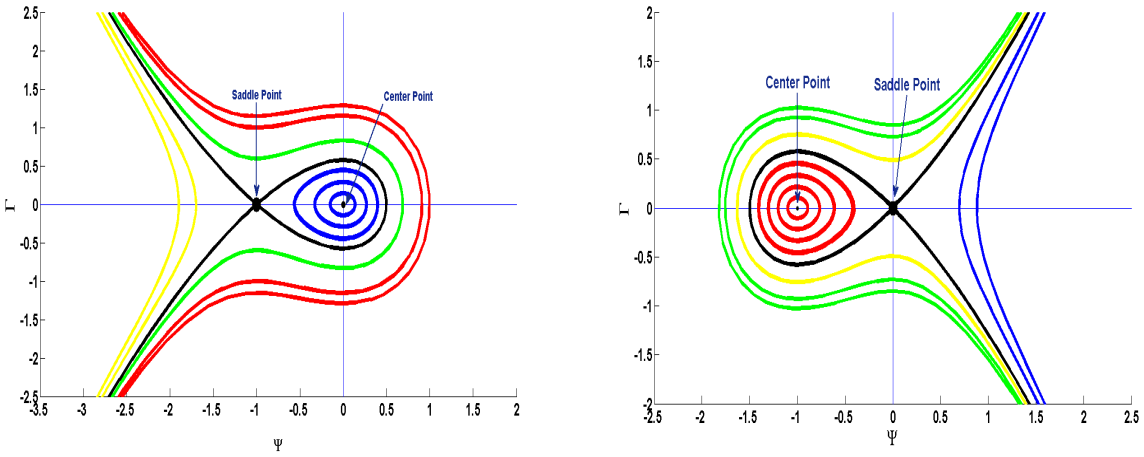

(a) a **(b)** b

Figure 10. Phase plots for (5.1), when (a): $\varpi_0 > 0$ and $\varpi_1 > 0$, (b): $\varpi_0 < 0$ and $\varpi_1 < 0$.

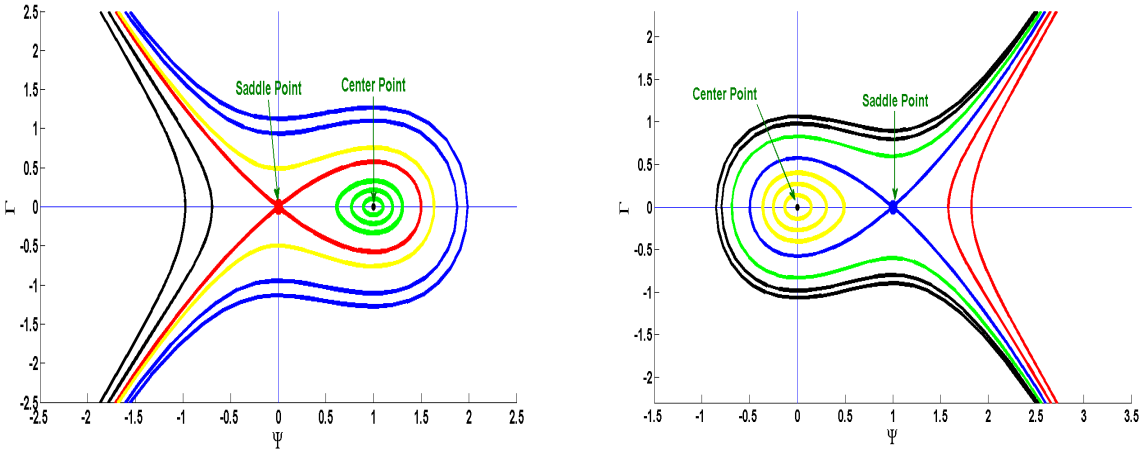

(a) a **(b)** b

Figure 11. Phase plots for (5.1), when (a): $\varpi_0 < 0$ and $\varpi_1 > 0$, (b): $\varpi_0 > 0$ and $\varpi_1 < 0$.

6. Chaotic phenomena

In this segment, we introduce an outward periodic force into system (5.1) to examine the dynamics of both quasi-periodic and chaotic phenomena [32, 33]. The modified system can be expressed in the following manner:

$$\begin{cases} \frac{d\Psi}{d\zeta} = \Gamma, \\ \frac{d\Gamma}{d\zeta} = -\varpi_0\Psi - \varpi_1\Psi^2 + \kappa_0\cos(\mathcal{G}), \\ \frac{d\mathcal{G}}{d\zeta} = \theta. \end{cases} \tag{6.1}$$

The above system is autonomous with $\mathcal{G} = \theta\zeta$. In the modified system (6.1), the perturbing force is characterized by two components referred to as κ_0 and θ. In this context, κ_0 represents the amplitude, while θ signifies the frequency of the disturbed term introduced into the (5.1). We have systematically investigated the chaotic dynamics of (6.1) using various tools, including three-dimensional plots, time plots, two-dimensional plots, and Lyapunov exponent. To gain deeper insights into this phenomenon, we explore the influence of both amplitude κ_0 and frequency θ, while maintaining the remaining parameters constant at $\varpi_0 = 2.5$ and $\varpi_1 = 1$ throughout our analysis.

In Figures 12(a)–14(a), time plots, two and three dimensional plots are presented by selecting $\kappa_0 = 0.02$ and $\theta = 0.03$. Under these parameter values, the system (6.1) exhibits periodic behavior. Subsequently, a slight adjustment is made to these parameters, setting them to $\kappa_0 = 1.3$ and $\theta = \pi$. Under these modified parameters, the system (6.1) exhibits quasi-periodic behavior, as visually depicted in Figures 12(b)–14(b). Continuing our analysis, the amplitude is further increased to $\kappa_0 = 3.7$, and the frequency is raised to $\theta = 2\pi$. In this scenario, system (6.1) demonstrates increased irregularity, revealing a quasi-periodic-chaotic nature, as illustrated in Figures 12(c)–14(c). Advancing further, the amplitude and frequency are adjusted to $\kappa_0 = 8.5$ and $\theta = 3\pi$. Under these values, system (6.1) exhibits heightened randomness, unveiling a chaotic nature as depicted in Figures 12(d)–14(d).

In the domain of dynamic systems, the Lyapunov exponent (LE) plays a crucial role in assessing the pace at which successive trajectories within a system develop independently. This scalar value, serves as a vital indicator of the system's inherent chaos. A positive LE denotes a chaotic state in the system, while a negative value indicates stability. In our analysis, we applied the Wolf method, incorporating Gram-Schmidt orthogonalization, to compute the LE for the scrutinized system. Subsequently, we visually represented the evolution of these exponents over time to gain insights into the dynamics of the system (6.1). In Figures 15 and 16, we illustrate the LE obtained against the temporal evolution, aiming to identify the chaotic phenomena of the modified system with parameters $\varpi_0 = 2.5, \varpi_1 = 1, \kappa_0 = 3.7, \theta = 2\pi$ and initial condition (0.05, 0.05, 0.05), (0.1,0.1,0.1). Similarly in Figures 17 and 18, the LE is presented with modified parameters as $\kappa_0 = 8.4, \theta = 3\pi$ and initial condition (0.3, 0.3, 0.3), and (0.5,0.5,0.5). This representation confirms the chaotic nature exhibited by the perturbed system (6.1).

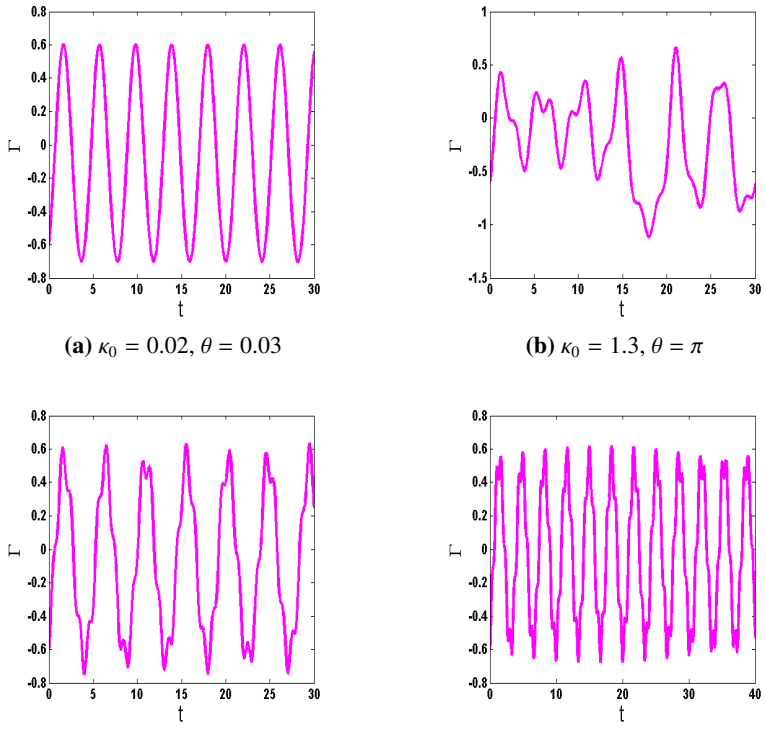

(a) $\kappa_0 = 0.02$, $\theta = 0.03$ **(b)** $\kappa_0 = 1.3$, $\theta = \pi$

(c) $\kappa_0 = 3.7$, $\theta = 2\pi$ **(d)** $\kappa_0 = 8.4$, $\theta = 3\pi$

Figure 12. Detection of chaotic phenomena in the perturbed system (6.1) via time plots.

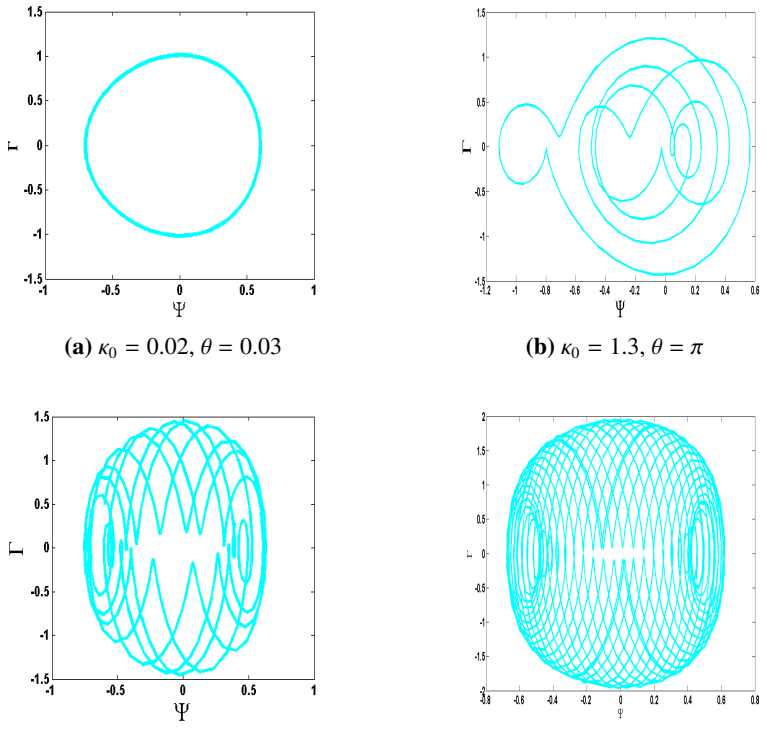

(a) $\kappa_0 = 0.02$, $\theta = 0.03$ **(b)** $\kappa_0 = 1.3$, $\theta = \pi$

(c) $\kappa_0 = 3.7$, $\theta = 2\pi$ **(d)** $\kappa_0 = 8.4$, $\theta = 3\pi$

Figure 13. Detection of chaotic phenomena in the perturbed system (6.1) via two dimensional plots.

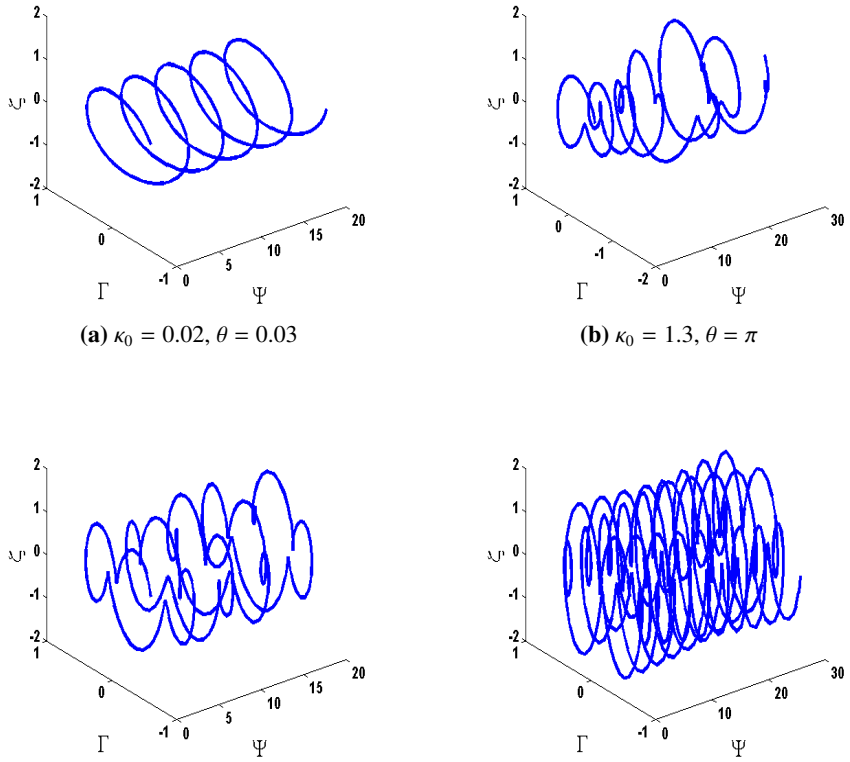

(a) $\kappa_0 = 0.02, \theta = 0.03$ **(b)** $\kappa_0 = 1.3, \theta = \pi$

(c) $\kappa_0 = 3.7, \theta = 2\pi$ **(d)** $\kappa_0 = 8.4, \theta = 3\pi$

Figure 14. Detection of chaotic phenomena in the perturbed system (6.1) via three dimensional plots.

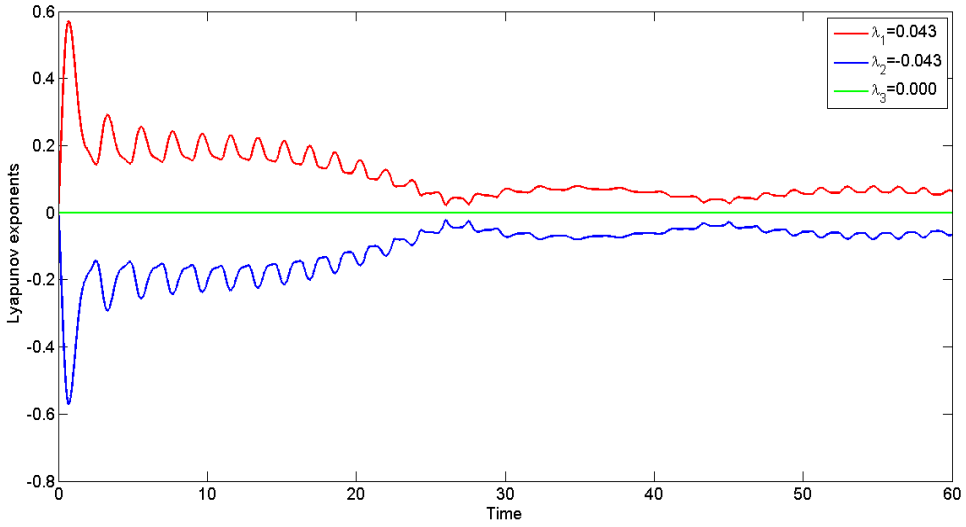

Figure 15. Detection of chaos in the system (6.1) via Lyapunov exponent with initial condition (0.05, 0.05, 0.05). $\varpi_0 = 2.5, \varpi_1 = 1, \kappa_0 = 3.7, \theta = 2\pi$.

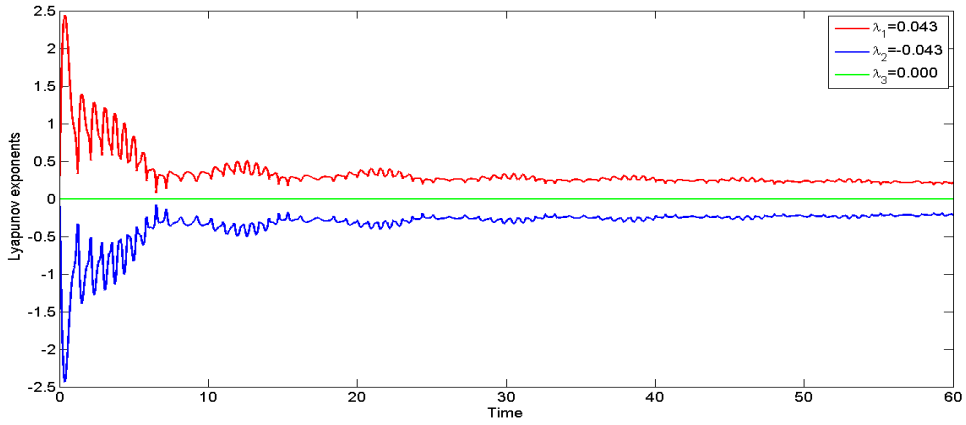

Figure 16. Detection of chaos in the system (6.1) via Lyapunov exponent with initial condition (0.1, 0.1, 0.1). $\varpi_0 = 2.5, \varpi_1 = 1, \kappa_0 = 3.7, \theta = 2\pi$.

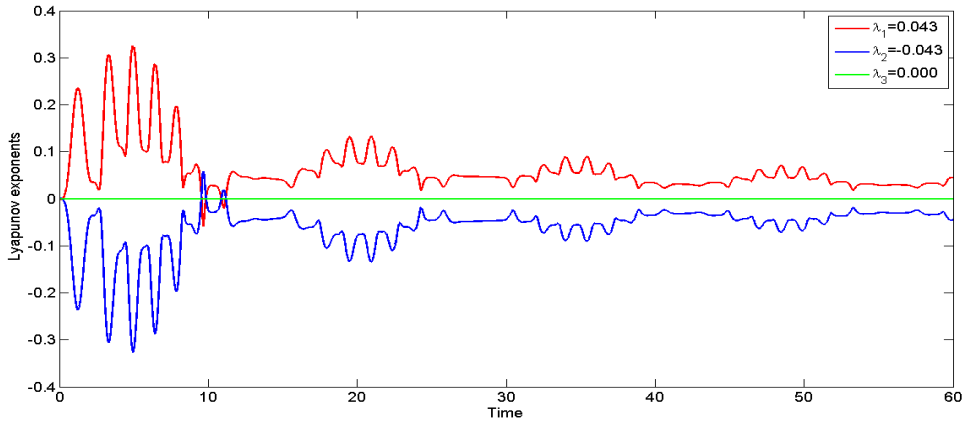

Figure 17. Detection of chaotic phenomena in the perturbed system (6.1) via Lyapunov exponent with initial condition (0.3, 0.3, 0.3). $\varpi_0 = 2.5, \varpi_1 = 1, \kappa_0 = 8.4, \theta = 3\pi$.

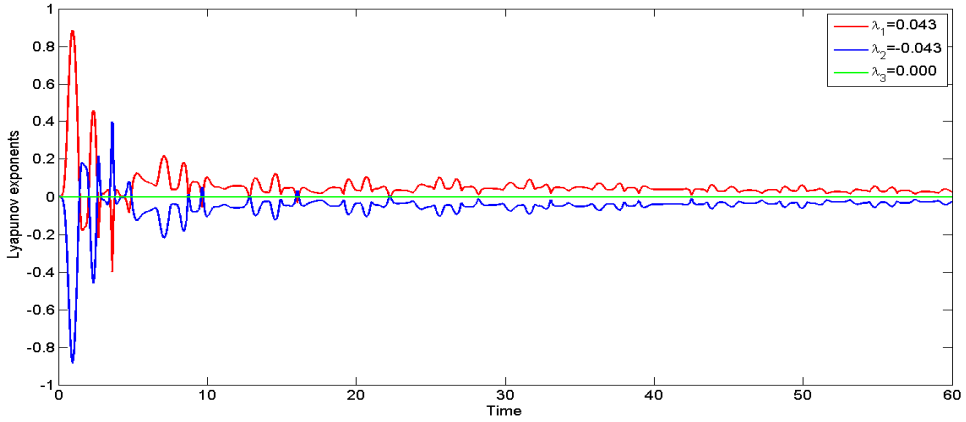

Figure 18. Detection of chaotic phenomena in the perturbed system (6.1) via Lyapunov exponent with initial condition (0.5, 0.5, 0.5). $\varpi_0 = 2.5, \varpi_1 = 1, \kappa_0 = 8.4, \theta = 3\pi$.

7. Sensitivity analysis

In this section, we explore the response of the suggested equation to variations in initial conditions. To assess the model's sensitivity, we examine four distinct sets of initial conditions. Figure 19 illustrates four solutions: $(\Psi, \Gamma) = (0.01, 0.01)$ in green, $(\Psi, \Gamma) = (0.03, 0.01)$ in red, $(\Psi, \Gamma) = (0.05, 0.01)$ in black, and $(\Psi, \Gamma) = (0.07, 0.01)$ in blue. Additionally, Figure 20 displays four solutions: $(\Psi, \Gamma) = (0.01, 0.01)$ in green, $(\Psi, \Gamma) = (0.06, 0.06)$ in red, $(\Psi, \Gamma) = (0.2, 0.2)$ in black, and $(\Psi, \Gamma) = (0.3, 0.3)$ in blue. It is apparent that even slight variations in the initial conditions can lead to subtle shifts in the dynamics of the system (5.1). Alternatively, we can assert that the two solution curves never overlap under any circumstances. Consequently, we infer that the proposed system exhibits sensitivity, though it is not excessively so.

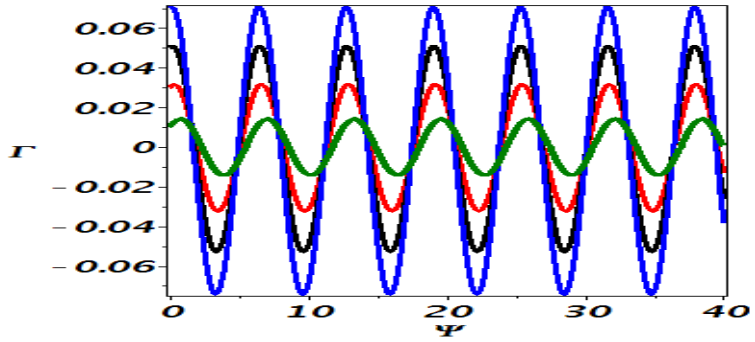

Figure 19. Sensitivity analysis across various initial values.

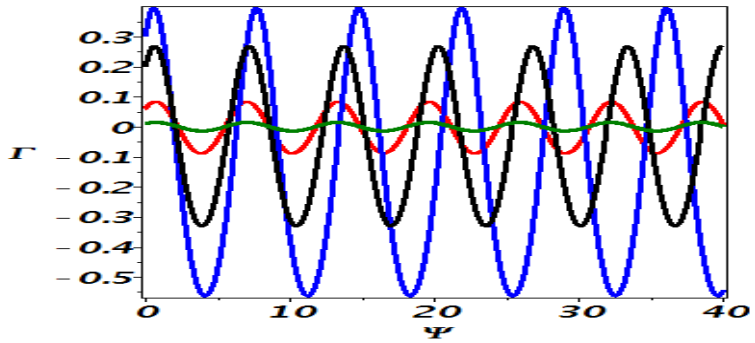

Figure 20. Sensitivity analysis across various initial values.

8. Conclusions

In brief, we delve into the extended integrable wave equation, a frequently employed concept in plasma physics, fluids, and various scientific fields. Our main concern is to conduct a thorough analysis of this equation, covering diverse facets such as the identification of solitons, examination of bifurcation phenomena, chaos analysis, and an investigation into the sensitivity of the proposed equation. At first, analytical solutions for the model under consideration were obtained using two effective and powerful approaches: the sub-equation approach and the Sardar sub-equation approach.

The suggested approaches offer a wide variety of solitons, such as bright, dark, combined dark-bright, and periodic solitary solitons. Bright and dark solitons are characterized by their distinctive intensity profiles; bright solitons exhibit a peak in intensity, whereas dark solitons display a dip. Additionally, dark-bright solitons combine both dark and bright features within their structure, featuring a localized region of decreased intensity (dark soliton) embedded within a localized region of increased intensity (bright soliton). Periodic soliton solutions demonstrate a repetitive structure.

Subsequently, an analysis of the dynamical nature of the model was undertaken, encompassing various aspects such as bifurcation, chaos, and sensitivity. Bifurcation has been examined at critical points, and the dynamical system, subjected to an outward periodic force, revealed chaotic phenomena. Chaotic behaviors has been illustrated through time plots, two-dimensional plots, three-dimensional plots, and the presentation of Lyapunov exponents, as illustrated in Figures 10)–18. The sensitivity analysis of the investigated model was executed utilizing the Runge-Kutta method. Future investigations into the extended integrable wave equation using alternative approaches remain a potential avenue for exploration. Thus, substantial research endeavors lie ahead to fully comprehend and explore the capabilities of this model. Such investigations hold promise for unveiling new insights and improving our comprehension of the behavior and characteristics of the discussed equation. Such advancements could potentially pave the way for the development of more precise and effective mathematical models and numerical techniques designed for solving this equation. The obtained findings indicate the efficacy of the presented approaches for analyzing phase portraits and solitons over a wider range of nonlinear systems.

Author contributions

Conceptualization, M.B.R. and A.J.; methodology, M.B.R. and A.J.; software, J.M. and M.B.R.; validation, S.S.K., M.B.R., and A.J.; formal analysis, M.B.R. and A.J.; investigation, M.B.R. and A.J.; data curation, S.S.K.; writing–original draft preparation, S.S.K.; writing–review and editing, M.B.R., J.M. and A.J.; visualization, M.B.R. and A.J.; supervision, A.J.; project administration, J.M. All authors have read and agreed to the published version of the manuscript.

Use of AI tools declaration

The authors declare they have not used Artificial Intelligence (AI) tools in the creation of this article.

Acknowledgments

This article has been produced with the financial support of the European Union under the REFRESH–Research Excellence For Region Sustainability and High-tech Industries project number CZ. 10.03.01/00/22_003/0000048 via the Operational Programme Just Transition.

Conflict of interest

The authors declare that they have no conflicts of interest.

References

1. S. Kumar, A. Kumar, B. Mohan, Evolutionary dynamics of solitary wave profiles and abundant analytical solutions to a (3+1)-dimensional burgers system in ocean physics and hydrodynamics, *J. Ocean Eng. Sci.*, **8** (2021), 1–14. https://doi.org/10.1016/j.joes.2021.11.002
2. N. Zobeiry, K. D. Humfeld, A physics-informed machine learning approach for solving heat transfer equation in advanced manufacturing and engineering applications, *Eng. Appl. Artif. Intel.*, **101** (2021), 104232. https://doi.org/10.1016/j.engappai.2021.104232
3. S. Kumar, S. Rani, N. Mann, Diverse analytical wave solutions and dynamical behaviors of the new (2+1)-dimensional Sakovich equation emerging in fluid dynamics, *Eur. Phys. J. Plus*, **137** (2022), 1226. https://doi.org/10.1140/epjp/s13360-022-03397-w
4. V. Jadaun, N. R. Singh, S. Singh, R. Shankar, Impact of solitons on the progression of initial lesion in aortic dissection, *Int. J. Biomath.*, **15** (2022), 2150096. https://doi.org/10.1142/S1793524521500960
5. V. Jadaun, A. Srivastav, A special phenomenon of wave interactions: an application of nonlinear evolution equation in (3+1)-dimension, *Commun. Nonlinear Sci. Numer. Simul.*, **130** (2024), 107733. https://doi.org/10.1016/j.cnsns.2023.107733
6. N. Raza, S. S. Kazmi, Qualitative analysis and stationary optical patterns of nonlinear Schrödinger equation including nonlinear chromatic dispersion, *Opt. Quant. Electron.*, **55** (2023), 718. https://doi.org/10.1007/s11082-023-04978-4
7. S. Duran, B. Karabulut, Nematicons in liquid crystals with Kerr Law by sub-equation method, *Alex. Eng. J.*, **61** (2022), 1695–1700. https://doi.org/10.1016/j.aej.2021.06.077
8. A. M. Wazwaz, Painlevé integrability and lump solutions for two extended (3+1)-and (2+1)-dimensional Kadomtsev-Petviashvili equations, *Nonlinear Dyn.*, **111** (2023), 3623–3632. https://doi.org/10.1007/s11071-022-08074-2
9. R. R. Yuan, Y. Shi, S. L. Zhao, J. X. Zhao, The combined KdV-mKdV equation: bilinear approach and rational solutions with free multi-parameters, *Results Phys.*, **55** (2023), 107188. https://doi.org/10.1016/j.rinp.2023.107188
10. S. S. Kazmi, A. Jhangeer, N. Raza, H. I. Alrebdi, A. H. Abdel-Aty, H. Eleuch, The analysis of bifurcation, quasi-periodic and solitons patterns to the new form of the generalized q-deformed Sinh-Gordon equation, *Symmetry*, **15** (2023), 1324. https://doi.org/10.3390/sym15071324
11. G. Akram, I. Zainab, M. Sadaf, A. Bucur, Solitons, one line rogue wave and breather wave solutions of a new extended KP-equation, *Results Phys.*, **55** (2023), 107147. https://doi.org/10.1016/j.rinp.2023.107147
12. M. A. Ullah, K. Rehan, Z. Perveen, M. Sadaf, G. Akram, Soliton dynamics of the KdV–mKdV equation using three distinct exact methods in nonlinear phenomena, *Nonlinear Eng.*, **13** (2024), 20220318. https://doi.org/10.1515/nleng-2022-0318
13. V. Jadaun, Soliton solutions of a (3+1)-dimensional nonlinear evolution equation for modeling the dynamics of ocean waves, *Phys. Scripta*, **96** (2021), 095204. https://doi.org/10.1088/1402-4896/ac0031

14. O. González-Gaxiola, A. Biswas, L. Moraru, A. A. Alghamdi, Solitons in neurosciences by the Laplace-Adomian decomposition scheme, *Mathematics*, **11** (2023), 1080. https://doi.org/10.3390/math11051080

15. B. Li, J. Zhao, W. Liu, Analysis of interaction between two solitons based on computerized symbolic computation, *Optik*, **206** (2020), 164210. https://doi.org/10.1016/j.ijleo.2020.164210

16. M. Sadaf, S. Arshed, G. Akram, E. Husaain, Dynamical behavior of nonlinear cubic-quartic Fokas-Lenells equation with third and fourth order dispersion in optical pulse propagation, *Opt. Quant. Electron.*, **55** (2023), 1207. https://doi.org/10.1007/s11082-023-05389-1

17. G. Akram, M. Sadaf, S. Arshed, M. Farrukh, Optical soliton solutions of Manakov model arising in the description of wave propagation through optical fibers, *Opt. Quant. Electron.*, **56** (2024), 906. https://doi.org/10.1007/s11082-024-06735-7

18. M. Vivas-Cortez, N. Raza, S. S. Kazmi, Y. Chahlaoui, G. A. Basendwah, A novel investigation of dynamical behavior to describe nonlinear wave motion in (3+1)-dimensions, *Results Phys.,* **55** (2023), 107131. https://doi.org/10.1016/j.rinp.2023.107131

19. S. Kumar, V. Jadaun, Symmetry analysis and some new exact solutions of Born-Infeld equation, *Int. J. Geom. Methods Mod. Phys.*, **15** (2018), 1850183. https://doi.org/10.1142/S0219887818501839

20. Y. Li, S. F. Tian, J. J. Yang, Riemann-Hilbert problem and interactions of solitons in the n-component nonlinear Schrödinger equations, *Stud. Appl. Math.*, **148** (2022), 577–605. https://doi.org/10.1111/sapm.12450

21. Z. Q. Li, S. F. Tian, J. J. Yang, E. Fan, Soliton resolution for the complex short pulse equation with weighted Sobolev initial data in space-time solitonic regions, *J. Differ. Equations*, **329** (2022), 31–88. https://doi.org/10.1016/j.jde.2022.05.003

22. Z. Q. Li, S. F. Tian, J. J. Yang, Soliton resolution for the Wadati-Konno-Ichikawa equation with weighted Sobolev initial data, *Ann. Henri Poincaré*, **23** (2022), 2611–2655. https://doi.org/10.1007/s00023-021-01143-z

23. Z. Q. Li, S. F. Tian, J. J. Yang, On the soliton resolution and the asymptotic stability of N-soliton solution for the Wadati-Konno-Ichikawa equation with finite density initial data in space-time solitonic regions, *Adv. Math.*, **409** (2022), 108639. https://doi.org/10.1016/j.aim.2022.108639

24. L. Akinyemi, Shallow ocean soliton and localized waves in extended (2+1)-dimensional nonlinear evolution equations, *Phys. Lett. A*, **463** (2023), 128668. https://doi.org/10.1016/j.physleta.2023.128668

25. A. M. Wazwaz, W. Alhejaili, S. A. El-Tantawy, Analytical study on two new (3+1)-dimensional Painlevé integrable equations: Kink, lump, and multiple soliton solutions in fluid mediums, *Phys. Fluids*, **35** (2023), 093119. https://doi.org/10.1063/5.0169763

26. N. Ullah, M. I. Asjad, A. Hussanan, A. Akgül, W. R. Alharbi, H. Algarni, et al., Novel waves structures for two nonlinear partial differential equations arising in the nonlinear optics via Sardar-subequation method, *Ale. Eng. J.*, **71** (2023), 105–113. https://doi.org/10.1016/j.aej.2023.03.023

27. D. Lathrop, Nonlinear dynamics and chaos: with applications to physics, biology, chemistry, and engineering, *Phys. Today*, **68** (2015), 54–55. https://doi.org/10.1063/PT.3.2751

28. M. B. Riaz, A. Jhangeer, J. Martinovic, S. S. Kazmi, Dynamics and soliton propagation in a modified Oskolkov equation: phase plot insights, *Symmetry*, **15** (2023), 2171. https://doi.org/10.3390/sym15122171

29. M. H. Rafiq, N. Raza, A. Jhangeer, Dynamic study of bifurcation, chaotic behavior and multi-soliton profiles for the system of shallow water wave equations with their stability, *Chaos Soliton. Fract.*, **171** (2023), 113436. https://doi.org/10.1016/j.chaos.2023.113436

30. K. Hosseini, E. Hinçal, M. Ilie, Bifurcation analysis, chaotic behaviors, sensitivity analysis, and soliton solutions of a generalized Schrödinger equation, *Nonlinear Dyn.*, **111** (2023), 17455–17462. https://doi.org/10.1007/s11071-023-08759-2

31. A. M. Talafha, A. Jhangeer, S. S. Kazmi, Dynamical analysis of (4+1)-dimensional Davey Srewartson Kadomtsev Petviashvili equation by employing Lie symmetry approach, *Ain Shams Eng. J.*, **14** (2023), 102537. https://doi.org/10.1016/j.asej.2023.102537

32. L. Bai, J. Qi, Y. Sun, Further physical study about solution structures for nonlinear q-deformed Sinh-Gordon equation along with bifurcation and chaotic behaviors, *Nonlinear Dyn.*, **111** (2023), 20165–20199. https://doi.org/10.1007/s11071-023-08882-0

33. L. Yang, M. ur Rahman, M. A. Khan, Complex dynamics, sensitivity analysis and soliton solutions in the (2+1)-dimensional nonlinear Zoomeron model, *Results Phys.*, **56** (2024), 107261. https://doi.org/10.1016/j.rinp.2023.107261

AIMS Press